JOURNAL OF SOLID STATE CHEMISTRY 91, 1–15 (1991)

Sn–K, Pb–L_3, and Ba–L_3 EXAFS, X-Ray Diffraction and ^{119}Sn Mössbauer Spectroscopic Studies of Ordered MSnF$_4$ (M = Pb and Ba) Fluoride Ionic Conductors with the α-PbSnF$_4$ Structure

G. DENES*

Laboratory of Solid State Chemistry and Mössbauer Spectroscopy, Department of Chemistry and Laboratories for Inorganic Materials, Concordia University, 1455 De Maisonneuve Blvd. W., Montreal, Quebec, H3G 1M8, Canada;

AND Y. H. YU, T. TYLISZCZAK, AND A. P. HITCHCOCK

Institute for Materials Research, McMaster University, Hamilton, Ontario, L8S 4M1, Canada

Received May 10, 1990; in revised form September 7, 1990

The high performance fluoride ion conductors α-PbSnF$_4$ and BaSnF$_4$ have been studied using X-ray diffraction, ^{119}Sn Mössbauer spectroscopy, and EXAFS. X-ray diffraction shows the unit-cell is a tetragonally distorted fluorite-type, with ordering of the metals which results in a superstructure along the **c** axis. The Sn–K, Pb–L_3, and Ba–L_3 X-ray absorption spectra of α-PbSnF$_4$ and BaSnF$_4$ as well as model compounds (SnO, β-PbF$_2$, and BaF$_2$) have been recorded at 300 and 77 K. Analysis of the extended fine structure (EXAFS) of α-PbSnF$_4$ and BaSnF$_4$ indicates they have a similar local structure around the corresponding metal atoms with average nearest neighbor distances of R_{Sn-F} = 2.08(3) Å, R_{Pb-F} = 2.50(3) Å and R_{Ba-F} = 2.67(2) Å. The good agreement between the Pb–F and Ba–F distances derived from EXAFS with diffraction results and ion pair estimates indicates that the Pb and Ba ions determine the close-packing arrangement of the crystal structure. EXAFS shows that the local structure is much better defined around Pb and Ba than around Sn. This and the weak temperature dependence of the Sn–K EXAFS indicates a lower rigidity of next-neighbor fluorine shells around Sn than around Pb or Ba. In the α-PbSnF$_4$ structural type, the metal M (Pb or Ba) is in an eightfold coordination site similar to the cubic coordination in the fluorite-type, whereas Sn is in a unique SnF$_5$E pseudooctahedral coordination, with the lone pair E being stereoactive and making the materials strongly anisotropic. This is confirmed by the large quadrupole splitting observed in Mössbauer spectroscopy, Δ = 1.52(2) mm/s for α-PbSnF$_4$ and 1.52(1) mm/s for BaSnF$_4$. The mobile fluoride ions are probably disordered and widely spread over conduction paths, and they remain disordered even at low temperature when their long range motion is frozen. The structural results are discussed in relationship to proposed mechanisms for ionic conduction in these materials.

I. Introduction

In recent years, there has been a great deal of experimental and theoretical work on the ionic mobility in materials which crystallize in the fluorite-type structure. This interest has focused on their unusually high conductivity at temperatures which are several hundred degrees below their melting points. Among the fluorite type

* To whom correspondence should be addressed.

0022-4596/91 $3.00

MF_2 materials, β-PbF_2 is by far the best conductor (about five orders of magnitude better than CaF_2, SrF_2, or BaF_2). The conductivity of β-PbF_2 and BaF_2 can be boosted by substituting some Pb (Ba) with Sn(II); a substitution rate of 50% leads to an increase of the conductivity by three orders of magnitude, as shown in Fig. 1 (*1–3*). The fast ion properties of $PbSnF_4$ were first discovered by Réau *et al.* (*3*) and this material has remained, to date, the highest performance fluoride ion conductor.

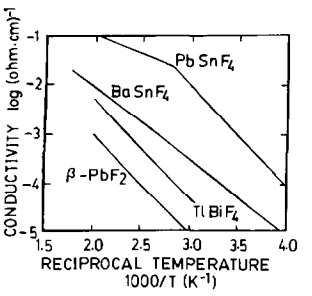

FIG. 1. Conductivity of MF_2 and $MSnF_4$ (M = Pb and Ba) (*1, 2*).

Detailed structural studies are required to understand the mechanism of fluoride ion mobility in these materials. The fluorite-type MF_2 compounds, and more particularly β-PbF_2, have been the subject of numerous X-ray and neutron diffraction studies. In contrast there have been relatively few studies of $MSnF_4$ compounds. Structural studies of α-$PbSnF_4$ and $BaSnF_4$ have been attempted by X-ray and neutron diffractions (*3–6*); however, these were not accurate enough: the R_N and R_{WP} residual factors were 0.079 and 0.119 for $BaSnF_4$ and 0.23 and 0.34 for α-$PbSnF_4$, respectively (*6*). One of the main reasons is that, to date, single crystals of sufficiently good quality cannot be obtained. Indeed, when α-$PbSnF_4$ is prepared from the reaction of $Pb(NO_3)_2$ and SnF_2 in aqueous solutions, very thin platelets (diameter/thickness > 100) are formed which are too thin to be collected. $BaSnF_4$ cannot be prepared by the same method using barium nitrate (*7, 8*). In addition, single crystals cannot be obtained from the melt, since both compounds decompose below their melting point (*9*). Therefore, most of the structural investigations have been limited to the study of powders. Because of the low scattering of X-rays by F, compared to Sn, Pb, and Ba, and also because of the strong preferred orientation exhibited by these materials, neutron diffraction is required to determine the fluoride ion positions. However, analysis of the neutron diffraction data is made difficult by the very strong texture (sheet structure) of the materials, which gives an inadequate line shape and line width for the Bragg peaks and results in the high residual factors given above (*6*). This problem was particularly severe in α-$PbSnF_4$ and precluded the refinement of the profile of its neutron powder pattern to a satisfactory R factor. However, isotypy of α-$PbSnF_4$ with $BaSnF_4$ could be confirmed. Since $PbSnF_4$ is to date the highest performance fluoride ionic conductor and previous structural studies were not fully successful, the use of a more appropriate technique for obtaining structural information is warranted. ^{19}F solid state NMR has also been performed and shows the presence of several kinds of fluoride ions, some mobile and others rigid (*2, 10*).

Ordinarily, the energy required to move an ion from one lattice site to another in a perfectly ordered crystal is prohibitively large. Ionic conduction in superionic solids is believed to be mediated by defects in the crystal structure, such as cation or anion vacancies in the lattice or displaced atoms, etc. (*11, 12*). EXAFS (extended X-ray absorption fine structure) has been a very useful probe of superionic conductors (*13–15*), because of its ability to probe the local structural environment of particular atom types in compound conductors. Analysis of the EXAFS spectra of normal and super-

ionic phases of several *cationic* conductors has revealed a great deal about the correlations between the highly mobile cations and the fixed anion lattice (*16*). Diffraction has been used previously to study the more heavily defective alkaline earth fluorides but it is inherently limited when applied to disordered solids as it provides only average structural information (*13–15*).

We have used X-ray diffraction, Mössbauer spectroscopy, and EXAFS to study the isotypic α-PbSnF$_4$ and BaSnF$_4$ compounds. X-ray powder diffraction provides the relationships between the lattice of MSnF$_4$ and β-PbF$_2$ and shows the type of lattice distortion and metal ordering present in the MSnF$_4$ compounds. Mössbauer spectroscopy establishes the tin hybridization and shows unambiguously that the tin(II) lone pair is stereoactive and electrically inactive, and that the tin site is highly distorted. EXAFS gives structural information about the metal sites (coordination, interatomic distances, and bond rigidity). The complementarity of the results from the three techniques is discussed in terms of structure/property relationships in the MSnF$_4$ ionic conductors.

II. Experiments, Materials, and Data Analysis

The chemicals used in the syntheses and/or as standards in the physical measurements were: PbF$_2$ 99.9%, from Alfa; BaF$_2$ from Baker & Adamson; SnF$_2$ 99.8% from Sharpe Chemical Co.; SnO powdered sample from OSI. α-PbSnF$_4$ was obtained by precipitation on addition of an aqueous solution of Pb(NO$_3$)$_2$ to a hot solution of SnF$_2$, according to a published procedure (*7, 8*). BaSnF$_4$ was prepared by reaction of solid BaF$_2$ with liquid SnF$_2$ at 500°C under dry nitrogen (*8, 9*). The reaction mixture was contained in a sealed copper tube as described in (*17*).

X-ray powder diffraction was carried out on a PW 1050-25 Philips diffractometer, using the Ni-filtered K_α radiation of copper (λ = 1.54178 Å). Tin-119 Mössbauer spectroscopy was performed using a Ca^{119m}SnO$_3$ γ-ray source from Amersham, an Elscint driving system working in the constant acceleration mode in the range −8 to +8 mm/s, and a Tracor Northern multichannel analyzer (Model TN 7200) operating in the multiscaling mode (*18*). The spectra were fitted on a CDC Cyber 835 main frame computer, using the GMFP5 program (*19*), which is a modified version of the GMFP software of Ruebenbauer and Birchall (*20*).

X-ray absorption spectra at the Sn–K (29.2 keV), Pb–L_3 (13.035 keV), and Ba–L_3 (5.247 keV) edges were recorded at the Cornell High Energy Synchroton Source (CHESS), in transmission mode. Details of the experimental procedures have been given previously (*21, 22*). Data processing was carried out with conventional Fourier filter and k-space curve-fit techniques (*23*) using both calculated spherical wave amplitude and phase functions (*24*) and experimental standards to derive distance, coordination number, and Debye-Waller ($\Delta\sigma^2$) information. k^1-weighting of the data was used.

III. Results and Discussion

3.1. Unit-Cell

Table I compares the unit-cell parameters of α-PbSnF$_4$ and BaSnF$_4$, determined by X-ray powder diffraction, to those of β-PbF$_2$ and BaF$_2$. The unit-cell of MSnF$_4$ is a tetragonal distortion of the fluorite-type (Fig. 2), such that the a and b parameters are equal to half the diagonal of the **a,b** face of fluorite and c is doubled. Since there are two MSnF$_4$ per unit-cell, compared to four MF$_2$ per unit-cell of fluorite, the change of volume is due only to the difference in ionic sizes and not to the lattice transformation. It should be pointed out that the origin of

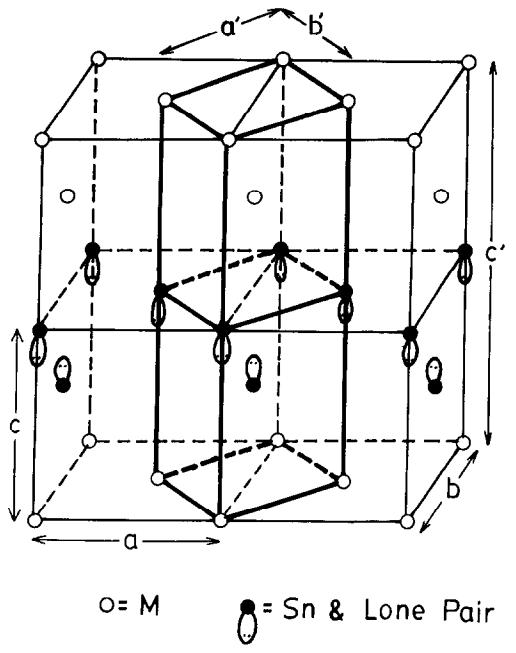

FIG. 2. Relationship between the unit-cells of MF_2 fluorite type (a, b, c) and $MSnF_4$ (M = Pb and Ba) (a', b', c'). The metal ions located on the front and the back (**a,c**) faces of the MF_2 cells have been omitted for clarity.

the unit-cell of $MSnF_4$ does not have to be on the metal site like in MF_2. The relationship between the unit-cells is clearly visible when one compares their X-ray powder diffraction patterns (Fig. 3), which can provide a hint about the structure of $MSnF_4$, as shown in the next paragraph. Four main changes are observed: (i) the tetragonal distortion causes a splitting of all (hkl) Bragg peaks with $l \neq h$; (ii) the 45° rotation of the axes in the (**a,b**) plane, with the $MSnF_4$ axes having half the length of the diagonals of the (**a,b**) face of MF_2, changes the h and k indices of all peaks except (001); (iii) the doubling of the **c** axis shows in the doubling of the l index; and (iv) the larger c parameter and lower symmetry (from $Fm3m$ to $P4/nmm$) makes new peaks appear. The combination of the four effects results in the following changes ($MSnF_4$ peaks are

TABLE I

UNIT CELL PARAMETERS OF $MSnF_4$ AND MF_2 (M = Pb AND Ba)

	M = Pb	M = Ba
MF_2:[a]		
a(Å)	5.940	6.2001
V(Å^3)	209.58	238.34
Z	4	4
Crystal system	Cubic	Cubic
Space group	$Fm3m$	$Fm3m$
$MSnF_4$:		
a(Å)	4.220(1)	4.3564(6)
c(Å)	11.415(3)	11.289(2)
V(Å^3)	203.3(1)	214.2(1)
$c/2a$	1.35	1.30
Z	2	2
Crystal system	Tetragonal	Tetragonal
Space group	$P4/nmm$	$P4/nmm$

Relationship of unit cell parameters of $MSnF_4$ and MF_2[b]

a	$a' = a/\sqrt{2}$
b	$b' = a'$
c	$c' = 2c$
V	$V' = V$
Z	$Z' = Z/2$

[a] The unit-cell parameters for the MF_2 fluorides were taken from [25 and 26].

[b] a, b, c, V, and Z (number of unit formulas in the unit-cell) refer to MF_2 and a', b', c', V' and Z' refer to $MSnF_4$.

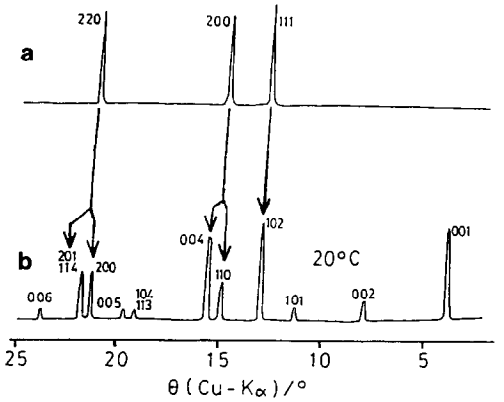

FIG. 3. Relationships between the X-ray powder pattern of (a) MF_2 fluorite type and (b) $MSnF_4$ (M = Pb and Ba).

primed):

—change of indexation and splitting of fluorite peaks,

(111) → (102)′

(200) → (100)′ and (004)′

(220) → (200)′ and (114)′

and

—the appearance of new peaks,

(001)′, (002)′, (101)′, (113)′, (104)′, (005)′, (201)′, and (006)′.

3.2. Interatomic Distances and Atomic Coordination

The unit-cell analogy between $MSnF_4$ and MF_2 fluorite-type strongly suggests a close relationship between the two structures. The symmetry reduction from cubic to tetragonal, the loss of the F lattice translation and the doubling of the c parameter indicate that M and Sn are most likely ordered in the **c** direction, although other reasons cannot be ruled out with certainty at this point. Tin-119 Mössbauer spectroscopic results (Table II) show that the parameters for α-$PbSnF_4$ and $BaSnF_4$ are very similar to those observed in α-SnF_2 (*27*). The large quadrupole splitting (Fig. 4) is characteristic of a significant p_z contribution to the lone pair of tin(II), which is $5s^{2-x}5p^x$ hybridized. This situation, similar to that encountered in α-SnF_2 and in all other known tin(II) fluoride containing compounds, is characteristic of a lone pair that is strongly stereoactive and which occupies an apex of the coordination polyhedron of the tin atom, as defined by Gillespie

TABLE II

^{119}Sn Mössbauer Spectroscopic Results for α-$PbSnF_4$ and $BaSnF_4$ at 298 K. Results for α-SnF_2 and $CsSnBr_3$ Are Presented for Comparison

Compound	δ(mm/s)[a]	Δ(mm/s)	Ref.
α-$PbSnF_4$	3.25(1)	1.52(2)	This work
$BaSnF_4$	3.255(6)	1.52(1)	This work
α-SnF_2	3.430(3)	1.532(3)	(*27*)
$CsSnBr_3$	3.93	0	(*28*)

[a] Isomer shifts are references to $CaSnO_3$ as zero shift at 298 K.

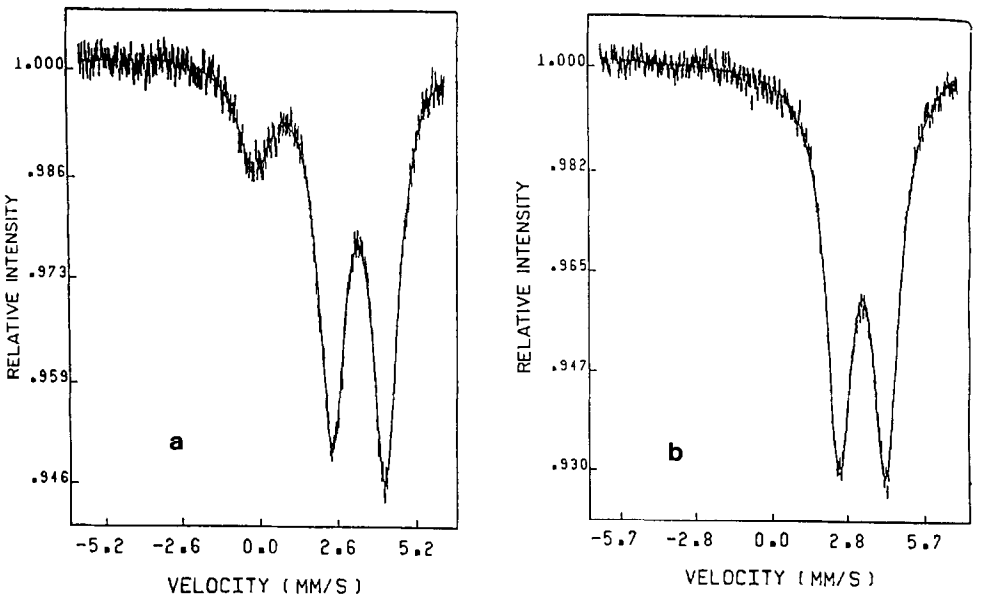

FIG. 4. ^{119}Sn Mössbauer spectrum of (a) α-$PbSnF_4$ and (b) $BaSnF_4$ at 298 K.

and Nyholm (*29*), Galy *et al.* (30), and Brown (*31*). This results in a strong distortion of the coordination of divalent tin, which cannot be similar to the cubic coordination of Pb and Ba in β-PbF_2 and BaF_2. This forces Sn and Pb/Ba to order. This strongly contrasts with $CsSnBr_3$, which has the perovskite structure with a regular octahedral coordination of tin(II). This is possible only because, in the latter case, the tin(II) lone pair is unhybridized, i.e., it has a purely *s* ($5s^25p^0$) spherical distribution, and therefore tin can take a regular highly symmetrical environment. In such cases, the larger *s* electron density gives a much more positive isomer shift, and the absence of *p* electron density, together with the regular environment, result in a zero quadrupole splitting (Table II). Such a situation, which is not found in α-$PbSnF_4$ and $BaSnF_4$, would be required for tin(II) to take a cubic coordination like Pb and Ba. The lattice obtained from X-ray diffraction is shown in Fig. 2. The Mössbauer spectroscopic results indicate that Pb and Sn cannot have similar coordinations, therefore they must be ordered, unless there is local site distortion like in $PbSn_4F_{10}$ (*18*). If Pb and Sn were not ordered, there would be no reason to lower the symmetry and create a supercell when going from MF_2 to $MSnF_4$ [see the case of $PbSn_4F_{10}$ (*18*)]. The only way to order Pb and Sn in the lattice observed by X-ray diffraction, for the same overall cationic sublattice as that found in fluorite, is that shown in Fig. 2. This type of order consists of two planes of Sn parallel to (**a,b**) alternating with two planes of Pb, also parallel to (**a,b**). Therefore, the metal ions are ordered along **c** according to the following sequence:

. . . Pb Pb Sn Sn Pb Pb . . .

Another experimental observation corroborates the above model: the crystal habit (very thin plates perpendicular to **c**) described in the introduction shows that extremely strong cleavage occurs between planes parallel to (**a,b**), and between these planes, bonding is quasi-nonexistent. Bridging Pb–F–Pb bonds are strong in all directions in the isotropic fluorite-type; therefore the lone pairs from the tin(II) atoms, which are always pointed in a direction opposite to the bonds, must preclude bonding between the two adjacent tin layers. Symmetry conditions force the lone pairs to be oriented parallel to **c**, otherwise each of them would be repeated by the fourfold axis (space group *P4/nmm*) and each tin would have four lone pairs. On the other hand, when the lone pair of each tin is oriented parallel to **c**, its multiplicity is the same as that of tin and only one lone pair per tin(II) is obtained after applying the

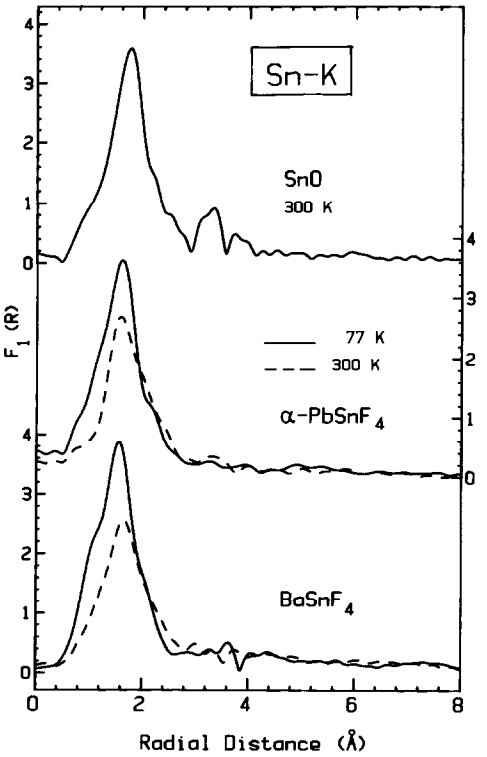

FIG. 5. Magnitudes of the Fourier transforms of the Sn–K EXAFS of SnO (300 K), α-$PbSnF_4$ and $BaSnF_4$ recorded at 77 and 300 K. A common vertical scale is used throughout.

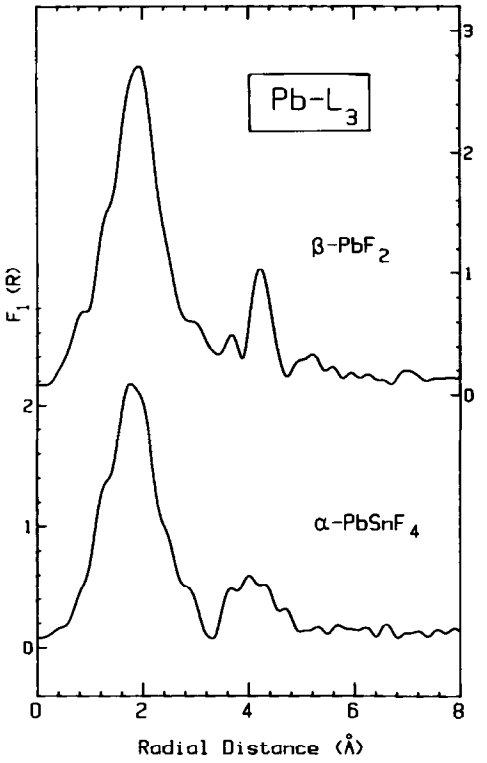

FIG. 6. Magnitude of the Fourier transforms of the Pb–L_3 EXAFS of β-PbF_2 and α-$PbSnF_4$ recorded at 300 K. See Table III for a summary of the k-ranges used in the transform as well as derived parameters.

symmetry conditions of the space group. Furthermore, the lone pairs belonging to the tin(II) atoms of one plane must point toward the adjacent tin(II) layer to make Sn–F–Pb bridges possible.

The information obtained from X-ray powder diffraction and Mössbauer spectroscopy is corroborated and supplemented by neutron powder diffraction (*6*) and EXAFS. The Fourier transform (FT) magnitudes of the k^1-weighted Sn–K, Pb–L_3, and Ba–L_3 EXAFS of α-$PbSnF_4$, $BaSnF_4$, and related models are presented in Figs. 5, 6, and 7, respectively. The average M–F first shell distances and coordination numbers are presented in Table III in comparison with diffraction results where these are available. The wave number range transformed and the radial distance ranges used for reverse transform (Fourier filter) analysis are summarized in Table III. Quantitative average M–F distances have been derived using phase and amplitude functions from spherical wave calculations (*24*) and experimental models. β-PbF_2 and BaF_2 have been used as experimental Pb–F and Ba–F standards since they have similar local structure and similar Pb–L_3/Ba–L_3 edge shape to α-$PbSnF_4$ and $BaSnF_4$. Stannous fluoride SnF_2 is unsuitable as an Sn–F EXAFS standard since the monoclinic polymorph, which is the only stable phase at 300 K (*33*), contains two types of Sn atoms, each with a different type of coordination and a range of fluorine near neighbors

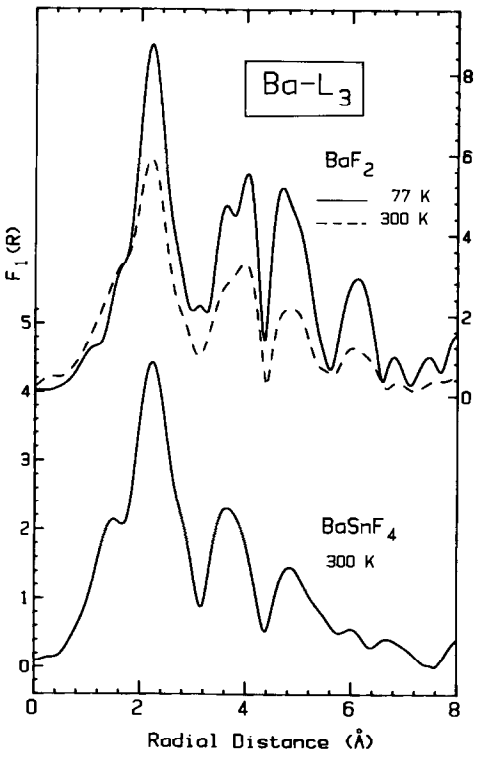

FIG. 7. Magnitudes of the Fourier transforms of the Ba–L_3 EXAFS of BaF_2 (77 and 300 K) and $BaSnF_4$ (300 K only).

TABLE III

COMPARISON OF INTERATOMIC DISTANCES AND COORDINATION NUMBERS DERIVED FROM EXAFS WITH DIFFRACTION RESULTS

			EXAFS[a]							
			Expt					Diffraction[b]		
Species	T(K)	Calculated R(Å)	R(Å)	N	$\sigma^2(10^{-3}Å^2)$	R^c	k^d	$d(M-X)$(Å)	N	Ref.
			Sn–F distances (Sn–K)							
α-$PbSnF_4$	300	2.10(3)	2.11(2)	—	5.2	0.8–3.0	3.6–11.2			
	77	2.11(1)	2.12(2)	4.3	2.2	0.6–3.0	3.2–11.4			
$BaSnF_4$	300	2.06(1)	2.08(3)		16.5	0.6–2.8	3.2–12.6	2.029(4)	1	(*6*)
								2.282(1)	4	(*6*)
	77	2.02(2)	2.07(2)	6.4	11.9	0.6–2.8	3.2–12.6			
SnO	300	2.22(1)	—	(4)	3.8[e]	0.8–3.0	2.5–14.5	2.22(2)	4	(*32*)
			Pb–F distances (Pb–L_3)							
α-$PbSnF_4$	300	2.45(3)	2.55(3)	6.6	14.2	0.6–3.0	2.1–11.9			
β-PbF_2	300	2.47(3)	—	(8)	13.4[e]	0.6–3.0	3.2–12.0	2.578	1	(*25*)
			Ba–F distances (Ba–L_3)							
$BaSnF_4$	300	2.65(3)	2.68(2)	4.6	8.5	1.0–4.0	2.0–9.8	2.626(1)	4	(*6*)
								2.955(2)	4	(*6*)
								3.148(1)	4	(*6*)
BaF_2	300	2.67(2)	2.66(2)	7.2	4.6	1.2–4.2	2.5–9.8	2.68	8	(*25*)
	77	2.65(1)		(8)	4.2					

[a] EXAFS results (first shell average M–X distance, errors are statistical only and do not incorporate systematic errors such as those associated with phase transferability or accuracy of calculated phase functions). Calculated R: distances derived using spherical wave calculated phases (*24*). Experimental distances: coordination number, and Debye–Waller parameters derived using experimental phase and amplitude models from the first shell Sn–K EXAFS of SnO (300 K), Pb–L_3 EXAFS of β-PbF_2 (300 K), and the Ba–L_3 EXAFS of BaF_2 (300 K). N: coordination number (±20%).

[b] Diffraction results: $d(M-X)$: M–X distances in Å (M = Sn, Pb or Ba; X = F or O); N: coordination number; Ref, reference number.

[c] R, range used for Fourier filtering.

[d] Range of wave number data Fourier transformed.

[e] DW derived using calculated amplitude functions (*24*).

(*34*). Instead, SnO was used as an experimental model for Sn–F phase and amplitudes. SnO has four equal Sn–O distances in a regular square pyramidal tin(II) coordination (*32*) with a well-defined first-shell EXAFS signal (Fig. 5). Such an "adjacent-Z" approximation is frequently used in EXAFS analysis and results in errors in radial distances of the order of 0.02 Å. The Sn–K EXAFS of SnO is in good agreement with that reported earlier by Yamaguchi *et al.* (*35*).

The FT magnitudes of the Sn–K EXAFS of α-$PbSnF_4$ and $BaSnF_4$ (Fig. 5) are dominated by a broad first-shell Sn–F signal with essentially no signal from more distance atoms, even at 77 K. The main effect on the EXAFS of increased temperature (77 → 300 K) is to broaden the main peak in the FT magnitude, although detailed analysis indicates that the Debye–Waller parameter does not change greatly with temperature (Table III). This suggests that the fluoride ions adopt a wider range of positions at

TABLE IV

SUMMARY OF M–F PARAMETERS DERIVED FROM MULTICOMPONENT ANALYSES OF FOURIER-FILTERED FIRST-SHELL EXAFS

Species	Edge	Model	Parameter	Component 1	Component 2	Component 3	Fit[a]
$BaSnF_4$ (300 K)	Sn–K	SnO—300 K	R (Å)	2.17	2.34		1.2
			N	2.3	3.1		
			$\Delta\sigma^2$ (10^{-3} Å^2)[b]	9.0	18		
			E_0	−8.5	0.3		
$PbSnF_4$ (300 K)	Sn–K	SnO—300 K	R (Å)	2.15	2.30		0.9
			N	1.9	1.3		
			$\Delta\sigma^2$ (10^{-3} Å^2)	−0.4	−1.3		
			E_0	−0.4	0.0		
$BaSnF_4$ (300 K)	Ba–L	BaF_2—300 K	R (Å)	2.68	2.90	3.31	1.7
			N	(0.5)[c]	(0.5)	(0.5)	
			$\Delta\sigma^2$ (10^{-3} Å^2)	−6.2	0.9	45	
			E_0	−1.5	−4.0	−4.0	

[a] 10^3 times the sum of the squares of the differences between calculation and Fourier-filtered experimental data.

[b] Difference on square of Debye–Waller term, relative to that of the model.

[c] Values fixed to the diffraction results during fit.

higher temperature (i.e., increased static disorder). Comparison of the Fourier magnitudes of the Sn-K EXAFS for α-$PbSnF_4$ and $BaSnF_4$ (Fig. 5) indicates that $BaSnF_4$ has a broader first shell peak and also a larger decrease in amplitude between 77 and 300 K. This suggests that $BaSnF_4$ has a wider range of Sn–F distances than α-$PbSnF_4$, even at lower temperatures.

The tin environment in $BaSnF_4$ obtained from neutron diffraction (*6*) consists of several closely spaced Sn–F distances which are not resolvable by EXAFS. We have used curve fit techniques to investigate the sensitivity of Sn–K EXAFS to this aspect of the structure. The results, based on the room temperature Sn–O first-shell EXAFS data as a model, are presented in Table IV and in Fig. 8. Although the fit quality is good and the two Sn–F distances derived are in reasonable agreement with those determined by diffraction, the relative numbers of each type of fluorine do not appear to be correctly reproduced. In addition the quality of the fit is not much better than that to a single component. A similar two-component curve fit analysis was carried out on the Fourier-filtered first-shell Sn–K EXAFS of $PbSnF_4$ (Table IV, Fig. 8) which the present results (diffraction, Mössbauer, and EXAFS) all suggest has a similar Sn local environment.

In contrast to the Sn–K EXAFS, which has an exclusively first-shell Sn–F signal, the Pb–L_3 and Ba–L_3 FT magnitudes (Figs. 6 and 7) exhibit considerable signals at higher distances (2.8–4.8 Å). In each case the dominant first shell Pb–F and Ba–F signals of the $MSnF_4$ compound are broader than that for the MF_2 standard, indicating a greater range of M–F distances from either thermal motion or static disorder. Unfortunately, the low temperature Pb–L_3 and Ba–L_3 spectra of the MSnF$_4$ species were not run in these cases so it is difficult to estimate the relative importance of these two factors.

The ionic radii (*36*) relevant to close-

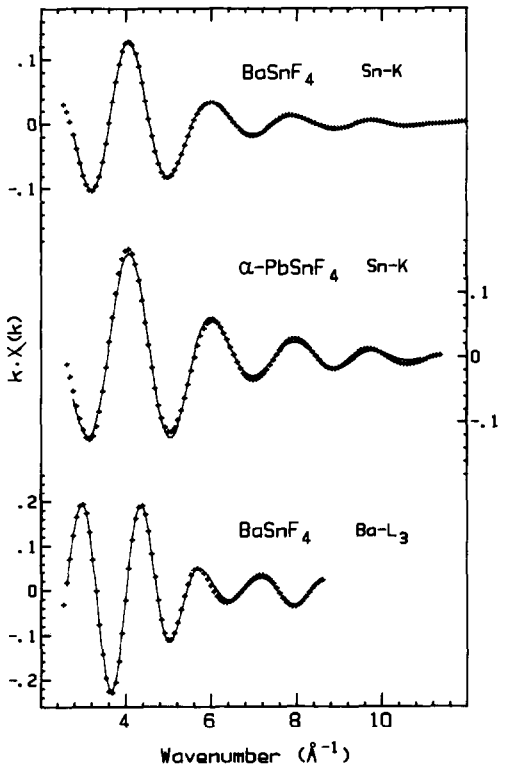

FIG. 8. Comparison of Fourier-filtered and curve-fit results for (a) first-shell Sn–F in $BaSnF_4$, (b) first-shell Sn–F in α-$PbSnF_4$, (c) first-shell Ba–F in $BaSnF_4$. See Table IV for a summary of the parameters.

packed ionic bonding between Sn–F, Pb–F and Ba–F pairs of atoms are listed in Table V in comparison with the average first-shell distances (for all species and all temperatures) derived from EXAFS. The agreement between the summed ionic radii and the *M*–F distances is excellent for both Pb–F and Ba–F but the EXAFS-derived first-shell average Sn–F distance is notably shorter than that predicted from ionic radii. This is not surprising since it has been shown that Sn–F bonds in divalent tin fluorides have a significant amount of covalency (*33, 34, 37, 38*). Partial overlap between the fluorine and the tin valence orbitals brings the two atoms closer to each other than would be expected for two hard

TABLE V

NEAREST NEIGHBOR DISTANCES PREDICTED FROM IONIC RADII COMPARED TO EXAFS RESULTS

	NN Distance (Å)	
Ion pair	Predicted[a]	Average (EXAFS)
Sn–F	2.26	2.08(3)
Pb–F	2.53	2.50(5)
Ba–F	2.67	2.67(2)

[a] The sum of ionic radii: F^- (1.33 Å), Sn^{2+} (0.93 Å), Pb^{2+} (1.20 Å), and Ba^{2+} (1.34 Å) (*36*).

shell ions held near each other by electrostatic attraction only.

In BaF_2, there are eight equal Ba–F distances of 2.68 Å (Fig. 9a). Ba is in the center of a F_8 cube and F is in the center of a regular Ba_4 tetrahedron (*39, 40*). In $BaSnF_4$, there are two groups of four equal Ba–F distances, 2.626 and 2.955 Å, respectively, and Ba is shifted toward one of the square faces of its polyhedron of coordination (Fig. 9b). There are four additional distances at 3.148 Å; however, these are only secondary weak bonding. Tin(II), which cannot take a cubic coordination because of its stereoactive lone pair, manages to fit in the quasicube network of BaF_2 units by binding to one face of the empty F_8 quasicubes, which are located between the BaF_8 quasicubes. The tin(II) lone pair is located

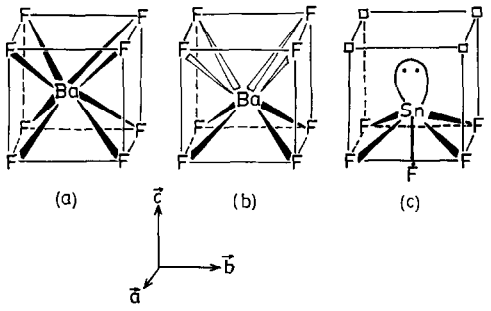

FIG. 9. Coordination of Ba and Sn in BaF_2 and $BaSnF_4$. (a) Ba in BaF_2, (b) Ba in $BaSnF_4$, (c) Sn in $BaSnF_4$; □ is a F vacancy.

on the opposite side of tin, and is clearly stereoactive, as shown by Mössbauer spectroscopy. The four fluorine atoms that would complete the SnF_8 cube if the lone pair was not stereoactive, have moved into empty F_8 cubes adjacent to tin, and on the opposite side of the lone pair, to form a short Sn–F axial bond. This results in a SnF_5E pseudooctahedral coordination of tin, with four equivalent equatorial bonds (Fig. 9c). This coordination, which has been described as the AX_5E configuration ℰ by Brown (*31*), has been observed in some Sb(III), Te(IV), I(V), and Xe(VI) compounds. However, it has not been found previously in tin(II), which seems to prefer lower coordination (AX_3E pseudotetrahedral and AX_4E pseudotrigonal bipyramidal). It should be noted that Sn(2) in α-SnF_2 takes a strongly distorted ℰ configuration with a short axial bond of 2.048 Å and four unequal equatorial bonds of 2.197, 2.276, 2.386, and 2.494 Å (*34*). A related and unique SnO_4E square pyramidal coordination of tin(II), with four equivalent equatorial bonds, but no axial bond, is found in black SnO (*32, 40*). The structure of $BaSnF_4$ contains three types of fluorine atoms: two of them are in a pseudotetrahedral coordination [F(1) in Ba_4F, and F(2) in Ba_2Sn_2F], whereas F(3) is in a terminal position and forms the short axial Sn–F bond.

The Ba–L_3 data were analyzed with k-space curve-fit techniques to see if EXAFS gave evidence for the multiple Ba–F distances. These results are summarized in Table IV and Fig. 8. In this case the derived distances are in good agreement with the values determined by neutron diffraction. As with the Sn–K curve-fit results, 1-component, 2-component, and 3-component fits were of similar quality so a unique answer is not provided. Tressaud *et al.* (*41*) have recently reported a Ba–L_3 and Mn–K EXAFS study of $Ba_{1-x}Mn_xF_2$ ionic conductors. As in this work, the disorder in the M–F distances gave difficulties in determining a unique local structure from EXAFS alone. As in the present work, the environment of the larger cation is less disordered.

3.3. Structure and Fluoride Ion Mobility

$MSnF_4$ is made of double layers of MF_8 quasicubes sandwiched between two layers of $SnF_4F'E$ pseudooctahedra (F = equatorial fluorines, F′ = axial fluorine, E = lone pair). Its structure is closely related to the fluorite type with the two main differences being: (i) tin and lead are ordered along the c axis as follows: . . . Pb Pb Sn Sn Pb Pb Sn Sn . . . , as suggested by the lattice obtained from X-ray diffraction, and (ii) the fluorine layer which would normally be between the two adjacent tin layers is absent; the fluorine atoms that would have made that layer have moved to non-occupied F_8 cubes adjacent to tin and form the axial Sn–F bond (*6*). Figure 10 shows that the replacement of half the Ba of BaF_2 by Sn to give $BaSnF_4$ results in a change from a three-dimensional $-[F_2\ Ba]_n-$stacking sequence to the highly layered structure [E Sn F_2 (F Ba) F_2 (Ba F) F_2 Sn E], with E being the tin(II) lone pair, and where the atoms enclosed by parentheses, i.e., (F Ba) and (Ba F), are nearly coplanar. The structural layers have no bonding interactions between them since they are separated by the tin(II) nonbonding pairs and the fluorine layer that should connect them has moved inside the two adjacent layers to form terminal axial bonding to tin. This explains the sheet texture of the crystallites and the high anisotropy of these materials.

The Sn–K EXAFS amplitudes are not strongly temperature dependent between 77 and 300 K, as indicated by the small Debye–Waller factor variation. These results are consistent with previous studies of α-$PbSnF_4$ and $BaSnF_4$ (*3–5*). First, Pb substitution for Sn reduces the symmetry of the fluorite structure causing increased disorder of the fluorite crystal structure as evidenced by the broadening of the nearest

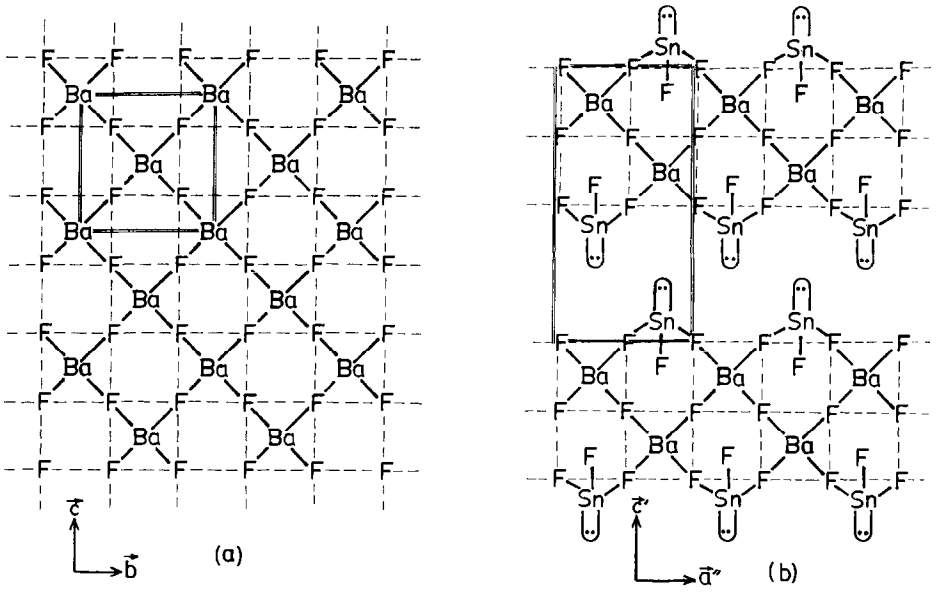

FIG. 10. Projection of the structure of (a) BaF_2 on the (**b**,**c**) plane, and (b) $BaSnF_4$ on the (**a**″,**c**′) plane (**a**″ = **a**′ + **b**′). The F_8 cubes/quasicubes are represented by dashed lines. The double lines indicate the unit-cell.

neighbor (NN) peak in the EXAFS. Second, the absence of significant temperature dependence in EXAFS seems to be in contradiction with ^{19}F NMR (*10*), which clearly shows the presence of two kinds of fluorine atoms, one highly mobile, the other stationary at 300 K, whereas no fluorine is mobile at low temperature (120 K). To reconcile the results from the two techniques, one has to remember that NMR studies of dipolar effects probe ionic motion, whereas in diffraction and EXAFS techniques, strong correlations occur between motional and static disorder effects. Diffraction studies of MF_2 fluorides have shown the presence of a considerable amount of disorder on the fluoride sublattice in the superionic phase (*42, 43*). Therefore, one can reasonably assume that the $MSnF_4$ compounds, with structures derived from the fluorite type, also have disordered fluoride ion sublattices. In addition, the much larger conductivity of $MSnF_4$ probably implies a much higher degree of disorder. This is the most probable cause for the poor agreement between diffraction results and the predictions of models in which all fluorine atoms are in fixed lattice positions, well coordinated to Sn and Pb/Ba. At least some of the disordered fluoride ions, if they are easily mobile, are on loosely defined sites, spread over conducting paths, and therefore are not directly associated with particular metal atoms. The absence of well-defined interstitial sites for fluoride ions in β-PbF_2 has been demonstrated from variable temperature X-ray diffraction (*5, 42, 43*). At any instant some of the tin atoms have less fluoride ions than expected in an ideal structure. The small temperature dependence of the EXAFS indicates that the uncertainties in the structure are much more related to static disorder than thermal motion, i.e., the more mobile ions are the disordered ones, and since the disordered ones are hardly detected by EXAFS,

whether they are moving or stationary makes little difference to the EXAFS spectrum. This is consistent with the NMR results (*10*), which show that there is very little exchange between mobile and nonmobile fluorines.

The good agreement between the Pb–F and Ba–F EXAFS-derived distances with the ion pair estimates (Table V) indicates that Pb and Ba are the elements which determine the close-packing arrangement of the crystal structure. Also, EXAFS shows that the environment is much better defined around Pb and Ba than around Sn (i.e., there is a narrower NN distribution, and higher (M–M) distances are clearly discerned in the FT magnitude of the Ba–L_3 and Pb–L_3 EXAFS but not the Sn–K EXAFS).

The high ionic mobility in the fluorite-type structure has been traditionally attributed to their ability to accommodate Frenkel defects, i.e., a combination of F vacancies and F interstitials, the interstitial sites being inside the empty F_8 cubes. The presence of one kind of F inside the F_8 quasicubes of $BaSnF_4$ could explain the large increase of F mobility, provided the exchange from axial F to equatorial F is easy. However, the axial Sn–F bond is clearly shorter than the sum of the Sn^{2+} and F^- ionic radii. Therefore it contains a significant degree of covalency, and most likely is difficult to break. In addition, the Frenkel defects model does not apply very well to $BaSnF_4$ since all F_8 quasicubes not occupied by a Ba are occupied by a terminal fluorine. Furthermore, Frenkel defects do not explain why the conductivity of β-PbF_2 is much higher than that of BaF_2, when the latter has clearly more space in its empty F_8 cubes for hosting interstitial fluoride ions. The higher polarizability of Pb(II) has been held responsible for the enhanced fluoride mobility of β-PbF_2. Similarly, the high polarizability of Sn(II) could explain the high conductivity of SnF_2 (*44*), since there are no empty sites in SnF_2 to allow for a high concentration of Frenkel defects. The above considerations do not lead to clear structural reasons for the superionic conductivity of the MSnF$_4$ materials. Since they have no empty F_8 cubes to host interstitial fluoride ions, the high polarizability of tin(II) is most likely one of the main factors involved, together with the remarkable ability of the MSnF$_4$ structure to accommodate a large amount of disorder on the anionic sublattice, and possibly other types of defects. The fact that the conductivity of α-$PbSnF_4$ is much higher than that of $BaSnF_4$ can be attributed to the presence of two highly polarizable cations, viz., Sn(II) and Pb(II).

Mössbauer spectroscopy also provides information about the conduction mechanism. One could postulate that the high conductivity of the MSnF$_4$ materials originates in the mobility of the tin nonbonded electron pair, which would make the compounds metallic conductors. However, the structure and the Mössbauer parameters show that the lone pair is located on a hybridized $5s^{2-x}5p^x$ orbital which is highly localized, since it is constrained to the valence shell of a single tin atom. This contrasts with compounds such as $CsSnBr_3$, with a nonhybridized nonbonded pair (*28*). The nonlocalized lone pair is easily detected by structural studies (regular coordination of tin) and by Mössbauer spectroscopy (high isomer shift, zero quadrupole splitting). This type of nonstereoactive lone pair can give rise to semiconducting properties, or even metallic conductivity, as was observed in $CsSnBr_3$ at high temperature, with transfer of the lone pair to the conduction band of the solid (*28*). The structure and Mössbauer spectrum of MSnF$_4$ clearly show that the tin lone pair in these materials is hybridized, stereoactive, and localized, and therefore cannot be a charge carrier. This is corroborated by transport number measurements, which show that F^-

ions are responsible for at least 99% of the total charge transport (*1*, *2*).

Summary

Even though α-$PbSnF_4$ and isotypic $BaSnF_4$ were reported first in 1967 and 1975, respectively, they resisted structural studies because of a combination of factors, including difficulties in growing single crystals, the high texture of the polycrystalline material, the presence of heavy metals, and the disorder on the fluoride sublattice. We have used a combination of structural techniques to investigate the local site and overall crystal structure of these fast ionic conductors.

X-ray powder diffraction has provided the unit-cell and shown that their structure derives from that of the fluorite type, with tetragonal distortion and order of the metals along the **c** axis of the cell. However, the strong texture and the presence of heavy atoms (Pb, Ba) made impossible the localization of fluorine atoms (the mobile species), and therefore hindered attempts to provide a static structural explanation of the mechanism of fluoride ion mobility.

Because neutron scattering factors do not increase with the square of the number of electrons, Pb, Ba, Sn, and F have comparable neutron scattering factors, and the light atom fluorine is not overshadowed by the heavy metals like in X-ray diffraction. Neutron powder diffraction (*6*) was successfully used for the localization of the fluoride ion sites and yielded the rigid polyhedra of coordination and packing. However, neutron powder diffraction, which is usually a very powerful technique, was limited here by the highly anisotropic shape of the crystallites and the disorder on the fluoride sublattice.

EXAFS and Mössbauer spectroscopy have provided information on local structural features. EXAFS shows that the MF_8 pseudocubes (M = Pb or Ba) are the building blocks of the $MSnF_4$ structures and are responsible for their analogy with the fluorite type. The disturbed environment of tin is underpopulated in fluorine, and the displaced fluorines are not ordered on specific crystallographic sites. According to previous ^{19}F NMR results (*10*), only the disordered fluoride ions are mobile, and there is no significant exchange with rigid fluorides. This is a major difference with MF_2 fluorides, in which the lattice fluorides undergo an appreciable shift to disordered positions at the superionic transition. This may explain the much higher conductivity of $PbSnF_4$ and $BaSnF_4$, which do not seem to exhibit such a transition.

Mössbauer spectroscopy provided the hybridization of tin(II) and the strong distortion of the tin site. In agreement with transport number measurements, it shows that the high electrical conductivity is not associated with mobile tin lone pair electrons. Indeed, the Mössbauer results show unambiguously that the tin nonbonding pair is stereoactive and highly localized in the immediate vicinity of tin.

Acknowledgments

This research has been financed by NSERC (Canada), the Ontario Centre for Materials Research, and the Quebec Ministry of Higher Education (MEST) under the Programme d'Actions Structurantes. A.P.H. and G.D. acknowledge the support of NSERC university research fellowships. The authors thank the staff of the Cornell High Energy Synchrotron Source (CHESS) for their assistance. CHESS is supported by the U.S. National Science Foundation.

References

1. G. Denes, T. Birchall, M. Sayer, and M. F. Bell, *Solid State Ionics* **13,** 213 (1984).
2. G. Villeneuve and P. Hagenmuller, *Phys. Status Solidi B* **97,** 295 (1980).
3. J. M. Réau, C. Lucat, J. Portier, P. Hagenmuller, L. Cot, and S. Vilminot, *Mater. Res. Bull.* **13,** 877 (1978).
4. G. Pérez, S. Vilminot, W. Granier, L. Cot,

C. LUCAT, J-M. RÉAU, J. PORTIER, AND P. HAGENMULLER, *Mater. Res. Bull.* **15,** 587 (1980).
5. S. PALCHOUDHURI AND G. K. BICHILE, *Solid State Commun.* **67,** 553 (1988).
6. T. BIRCHALL, G. DENES, K. RUEBENBAUER, AND J. PANNETIER, *Hyperf. Inter.* **29,** 1331 (1986).
7. J. D. DONALDSON AND B. J. SENIOR, *J. Chem. Soc. A,* 1821 (1967).
8. G. DENES, J. PANNETIER, AND J. LUCAS, *C.R. Acad. Sc. Paris C,* **280,** 831 (1975).
9. J. PANNETIER, G. DENES, AND J. LUCAS, *Mater. Res. Bull.* **14,** 627 (1979).
10. M. DURAND-LE FLOCH, J. PANNETIER, AND G. DENES, *Phys. Rev. B* **33,** 632 (1986).
11. S. P. VERNON AND M. B. STEARNS, *Phys. Rev. B* **29,** 6968 (1984).
12. "Fast Ion Transport in Solids, Electrodes and Electrolytes", (P. Vashita, J. N. Mundy, and G. K. Shenoy, Eds.), pp. 225–691, North-Holland (1979).
13. C. R. A. CATLOW, A. V. CHADWICK, G. N. GREAVES, AND L. M. MORONEY, *Nature (London)* **312,** 601 (1984).
14. C. R. A. CATLOW, A. V. CHADWICK, G. N. GREAVES, AND L. M. MORONEY, Proc. EXAFS III, (K. O. Hodgson, B. Hedman, and J. K. Penner-Hahn, Eds.), p. 435, Springer-Verlag (1984).
15. P. O. BATTLE, C. R. A. CATLOW, A. V. CHADWICK, G. N. GREAVES, AND L. M. MORONEY, Proc. EXAFS IV, *J. Phys. Coll.* **47,** C8-669 (1986).
16. T. M. HAYES AND J. B. BOYCE, *J. Phys. C* **13** L731 (1980); T. M. HAYES AND J. B. BOYCE, in "EXAFS and Near Edge Structure", Vol. 27, p. 182, (A. Bianconi, L. Incoccia, and S. Stipcich, Eds.), Springer Series in Chemical Physics (1984); A. YOSHIASA, F. KANAMARU, S. EMURA, AND K. KOTO, *Solid State Ionics* **27,** 267, 275 (1988); F. ROCCA, G. DALBA, AND P. FORNASINI, *Mater. Chem. Phys.* **23,** 85 (1989).
17. G. DENES, *J. Solid State Chem.* **77,** 54 (1988).
18. G. DENES, *J. Solid State Chem.* **74,** 343 (1988).
19. J. MONNIER, G. DENES, AND R. B. ANDERSON, *Canad. J. Chem. Eng.* **62,** 419 (1984).
20. K. RUEBENBAUER AND T. BIRCHALL, *Hyperfine Interact.* **7,** 125 (1979).
21. A. P. HITCHCOCK, C. J. L. LOCK, AND B. LIPPERT, *Inorg. Chim. Acta* **124,** 101 (1986).
22. Y. H. YU, T. TYLISZCZAK, AND A. P. HITCHCOCK, *J. Phys. Chem. Sol.* **51,** 445 (1990).
23. D. E. SAYERS AND B. A. BUNKER, Data Analysis, *in* "Chemical Analysis 92", (D. C. Koningsberg and R. Prins, Eds.), p. 211, Wiley, New York (1988).
24. A. G. MCKALE, B. M. VEAL, A. P. PAULIKAS, S.K. CHAN, AND G. S. KNAPP, *J. Amer. Chem. Soc.* **110,** 3763 (1988).
25. A. R. WEST, "Solid State Chemistry and Its Applications", p. 240, Wiley, New York (1984).
26. A. R. WEST, "Basic Solid State Chemistry", p. 35, Wiley, New York (1988).
27. T. BIRCHALL, G. DENES, K. RUEBENBAUER, AND J. PANNETIER, *J. Chem. Soc. Dalton Trans.,* 2296 (1981).
28. J. D. DONALDSON AND J. SILVER, *J. Chem. Soc. A,* 666 (1973).
29. R. J. GILLESPIE AND R. S. NYHOLM, *Q. Rev. Chem. Soc.* **11,** 339 (1957).
30. J. GALY, G. MEUNIER, S. ANDERSSON, AND A. ASTRÖM, *J. Solid State Chem.* **13,** 142 (1975).
31. I. D. BROWN, *J. Solid. State Chem.* **11,** 214 (1974).
32. J. PANNETIER AND G. DENES, *Acta Crystallogr. B* **36,** 2763 (1980).
33. G. DENES, *Mater. Res. Bull.* **15,** 807 (1980).
34. G. DENES, J. PANNETIER, J. LUCAS, AND J. Y. LE MAROUILLE, *J. Solid State Chem.* **30,** 335 (1979).
35. T. YAMAGUCHI, O. LINDQVIST, J. CLAESON, AND J. B. BOYCE, *Chem. Phys. Lett.* **93,** 528 (1982).
36. R. C. WEAST, Ed., "CRC Handbook of Chemistry and Physics," 61st ed., p. F-216, CRC Press, Boca Raton, FL (1980–1981).
37. G. DENES, J. PANNETIER, AND J. LUCAS, *J. Solid State Chem.* **33,** 1 (1980).
38. G. DENES, *J. Solid State Chem.* **36,** 20 (1981).
39. R. W. G. WYCKOFF, "Crystal Structures," Vol. 1, p. 432, Interscience, New York (1982).
40. A. F. WELLS, "Structural Inorganic Chemistry," 5th ed., p. 252–258, Oxford University Press, London/New York (1984).
41. A. TRESSAUD, G. DEMORTAIN, B. TANGUY, J. PORTIER, P. HAGENMULLER, H. DEXPERT, AND M. H. TUILIER, *J. Non-Cryst. Solids* **109,** 114 (1989).
42. K. KOTO, H. SCHULZ, AND R. A. HUGGINS, *Solid State Ionics* **1,** 355 (1980).
43. K. KOTO, H. SCHULZ, AND R. A. HUGGINS, *Solid State Ionics* **3/4,** 381 (1981); N. KAMIJO. K. KOTO, Y. ITO, K. TANABE, H. TERAUCHI, H. MUEDU, AND M. HIDU, in "EXAFS and Near Edge Structure III," p. 352, (K. O. Hodgson, B. Hedman, and J. E. Penner-Hahn, Eds.), Springer-Verlag, New York/Berlin (1984).
44. D. ANSEL, G. DEBUIGNE, G. DENES, J. PANNETIER, AND J. LUCAS, *Ber. Bunsenges. Phys. Chem.* **82,** 380 (1978).